



Application of inelastic X-ray scattering to the measurements of acoustic wave velocities in geophysical materials at very high pressure

G. Fiquet^{a,*}, J. Badro^a, F. Guyot^a, Ch. Bellin^a, M. Krisch^b, D. Antonangeli^b, H. Requardt^b, A. Mermet^b, D. Farber^c, C. Aracne-Ruddle^c, J. Zhang^d

^a *Laboratoire de Minéralogie Cristallographie, UMR CNRS 7590, Universités Paris VI et VII, Institut de Physique du Globe de Paris, 4 Place Jussieu, 75252 Paris, cedex 05, France*

^b *European Synchrotron Radiation Facility, BP220, 38043 Grenoble, cedex, France*

^c *Lawrence Livermore National Laboratory, Energy and Environment Directorate, 4000 East Ave., 94550 Livermore, CA USA*

^d *CHiPR and Department of Geosciences, SUNY Stony Brook, Stony Brook, NY 11794, USA*

Received 17 January 2003; received in revised form 29 September 2003; accepted 3 October 2003

Abstract

Reference Earth global models used by geophysicists are mostly constrained by analysing seismic waves that travel in the Earth. The interpretation of these seismological models in terms of chemical composition and temperature thus relies on the knowledge of the chemical composition, structure and elastic properties of some candidate materials relevant to geophysics. We will describe some recent advances in experimental mineral physics which yield essential information on the elastic properties of pertinent materials of Earth's mantle and core. In particular, we show that inelastic X-ray scattering (IXS) proves to be a well suited spectroscopic technique for the study of phonon dispersion in materials under high pressure. Inelastic scattering experiments carried out on polycrystalline samples provide measurements of orientationally averaged longitudinal acoustic velocities whereas investigations on single crystals yield elastic moduli. Such a technique is thus highly interesting for mineral physicists and offers a great potential in providing essential elastic data and their pressure and/or temperature dependence on most compounds of geophysical interest.

© 2004 Published by Elsevier B.V.

Keywords: Earth's interior; Mineral physics; High pressure; Physical properties; Elasticity; Techniques

1. Introduction

Knowledge of the elasticity of minerals is essential to the understanding and interpretation of seismic data, in particular radial average sound velocity profiles or

three dimensional images from tomographic studies. Successful interpretation of these seismic models in terms of chemical composition, mineralogy, and temperature indeed requires information on the elasticity of deep Earth materials under high pressure and temperature conditions. The experimental determination of elastic properties at extreme conditions is, however, not an easy task. Still, numerous experimental procedures have been developed during these last

* Corresponding author. Tel.: +33-14427-5236;

fax: +33-144-273785.

E-mail address: fiquet@lmcp.jussieu.fr (G. Fiquet).

decades, which couple high-pressure apparatuses to various techniques such as static (at zero frequency), shock-wave compression, or dynamical acoustic vibration (ranging from MHz to GHz frequency range). Among them, we mention the following:

- Shock measurements: measurements of the compressional wave velocities under shock compression along the Hugoniot in iron (Brown and McQueen, 1986), forsterite to 150 GPa (Duffy and Ahrens, 1992), periclase to 27 GPa (Duffy and Ahrens, 1995) or molybdenum to 81 GPa (Duffy and Ahrens, 1994).
- Resonant ultrasound spectroscopy to study the behaviour of minerals at extreme temperature and room pressure, e.g. single crystal periclase or forsterite to 1800 K (Isaak et al., 1989a,b).
- The implementation of ultrasonic interferometric measurements using a 1000 tonnes uniaxial split-cylinder apparatus (see Liebermann and Li, 1998) with applications to polycrystalline olivine to 10 GPa and 1300 K (Li et al., 1998), wadsleyite to 7 GPa and 873 K (Li et al., 2001) or MgSiO₃ perovskite to 8 GPa and 800 K (Sinelnikov et al., 1998).
- Optical probes using phonon–photon scattering processes with stimulated Brillouin scattering in a diamond–anvil cell with measurements of single crystal elastic moduli of natural samples of olivine, orthopyroxene and garnet to 20 GPa (Brown et al., 1989; Zaug et al., 1993; Chai et al., 1997a,b; Abramson et al., 1999).
- The extension of pressure range using conventional Brillouin spectroscopy with measurements on periclase to 55 GPa (Zha et al., 2000) or silica glass to 58 GPa (Zha et al., 1994). Data on periclase and synthetic pyrope to 20 GPa (Sinogeikin and Bass, 2000) as well as polycrystalline materials such as natural majorite-pyrope solid solution under pressure (Sinogeikin and Bass, 2002).

Furthermore, first-principles methods have been applied to the study of the high-pressure phases relevant to the Earth's deep interior such as MgSiO₃ perovskite (Karki et al., 2000; Oganov et al., 2001), hcp iron (Alfe et al., 2001; Steinle-Neumann et al., 2001) and hcp cobalt (Steinle-Neumann et al., 1999). The reader is invited to refer to the review articles by Stixrude et al. (1998) or Karki et al. (2001).

None of these methods provides unique answers to the standing long geophysical term requirement of obtaining precise measurements of compressional velocities V_P and shear velocities V_S , at extreme pressures and temperatures in chemically and mineralogically complex materials over a large frequency and wavelength range. This is why any technique bringing new information in this field is valuable. Recently, the use of X-ray diffraction (XRD; Mao et al., 1998; Matthies et al., 2001) and of several inelastic scattering techniques such as nuclear resonance inelastic X-ray scattering (NRIXS) (Lubbers et al., 2000; Mao et al., 2001), inelastic neutron (INS) (Klotz and Braden, 2000) and inelastic X-ray scattering (IXS) (Fiquet et al., 2001), have provided new data on geophysically relevant materials. In this paper, we will concentrate on the method of inelastic X-ray scattering with very high energy resolution ($\Delta E/E = 10^{-7}$) which has proven to be well suited for the determination of elastic properties of matter at high pressure (Krisch et al., 1997; Occelli et al., 2001) at THz frequencies. For geophysics, such high frequencies have the interest of getting close to the infinite frequency limit, in complementarity with the low frequency limit provided by radial X-ray diffraction modeling. IXS has more potential in ultra-high pressure geophysics (e.g. lower mantle and core) than INS which requires larger samples. Such INS experiments are therefore limited at present to pressures which do not exceed 10–15 GPa. Furthermore, INS technique is restricted to measurements of relatively low acoustic velocities in disordered or polycrystalline systems. IXS cross section is proportional to $f(Q)^2 Q^2 \rho/\mu$ where ρ is the specific volume, μ the absorption coefficient and Q the wave vector. The optimal signal for DAC experiments is obtained if the absorption length $t = 1/\mu$ is of the order of 10–40 μm , typically spanning elements with Z between 30 and 50. However, previous experiments have shown that studies on lower Z (Occelli et al., 2001; Krisch et al., 2002) and higher Z materials (Loa et al., 2003) are as well possible. Finally, we note that higher order Brillouin zones can be explored in single crystals, where the signal is enhanced by $f(Q)^2 Q^2$. In the following, examples of applications of IXS will be given for polycrystalline iron, iron alloyed with light elements, MgSiO₃ perovskite, as well as one example of cobalt single crystal.

2. Experimental setup

The development of IXS with meV energy resolution goes back to work at HASYLAB (Germany) in the 1980s (see Burkel et al. (1987) or Dorner et al., 1987). This method allows to study phonons and phonon-like excitations. The theoretical aspect will not be discussed here and the reader is referred to the articles of Schülke (1991) and Burkel (2000). The basic kinematics of the inelastic scattering process is described in Fig. 1. The incident photon of energy $\hbar\omega_1$ and wave vector \vec{k}_1 is scattered by the sample into a photon characterized by energy $\hbar\omega_2$ and wave vector \vec{k}_2 , a process corresponding to an energy transfer $\hbar\omega = \hbar\omega_1 - \hbar\omega_2$ and the momentum transfer $\hbar\vec{Q} = \hbar\vec{k}_1 - \hbar\vec{k}_2$. In the cases investigated in this study, the energy transfers are of the order of meV, much smaller than the incident photon energy of 15–25 keV, and Q is only controlled by the scattering angle theta, with the following expression:

$$Q = 2k_1 \sin\left(\frac{\theta}{2}\right) \quad (1)$$

At the ESRF (European Synchrotron Radiation Facility), two beamlines (ID16 and ID28) are dedicated to X-ray inelastic scattering spectroscopy. On ID28, the X-ray beam produced by three undulators

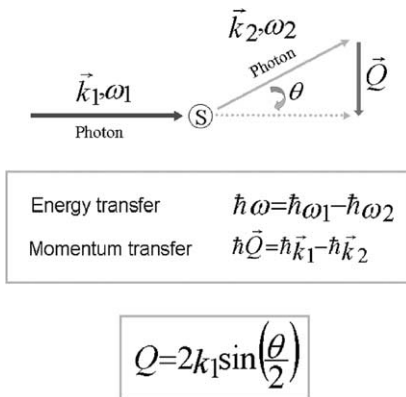


Fig. 1. Scattering geometry and kinematics of the inelastic scattering process. The incident X-ray photon characterized by angular frequency ω_1 and wave vector \vec{k}_1 , and scattered photon by angular frequency ω_2 and wave vector \vec{k}_2 . As long as the transferred energy is much smaller than the incident photon energy, the momentum transfer Q is simply connected with the geometry of the experiment, i.e. the scattering angle θ .

is monochromatized by a cryogenically cooled silicon (111) crystal and a high-energy resolution silicon backscattering monochromator (Verbeni et al., 1996). The backscattered beam is focused by a gold-coated toroidal mirror which provides a focal spot at the sample position of 250 μm (horizontal) by 60 μm (vertical) full-width-half-maximum. The scattered photons are analyzed by five analyzers mounted on a Rowland circle at a distance of 650 cm from the sample (Masciovecchio et al., 1996). The energy-analyzed photons are subsequently detected by a Peltier-cooled five element silicon diode detector positioned near the sample position 3 mm above the incident beam axis. According to Eq. (1), the momentum transfer Q is selected by rotating the spectrometer arm in the horizontal scattering plane around a vertical axis passing through the scattering sample (see Fig. 2). The energy scans are performed by varying the monochromator temperature while the temperature of the analyzers is kept fixed. With a linear thermal expansion of silicon at room temperature $\alpha = 2.58 \times 10^{-6} \text{ K}^{-1}$ and a conversion to the energy scale according to the relation: $\Delta E/E = \alpha \Delta T$, a temperature scan over a few degrees with mK resolution provides the necessary meV resolution in energy needed to probe phonon excitations. The sample orientation and scattering angle are kept fixed whereas the energy of the beam impinging on the sample is changed by varying the monochromator temperature in steps of 0.005–0.020 K over 1–4 K, corresponding to a scanning range of several 10 meV up to a few 100 meV.

In order to illustrate how data processing is made, a typical IXS spectrum is given in Fig. 3 for polycrystalline bcc iron at ambient conditions. On both sides of the elastic line centered at zero-energy transfer, one can notice two excitations which correspond to the scattering of incident X-ray photons by longitudinal acoustic LA phonons in iron. These Stokes (energy loss) and anti-Stokes (energy gain) inelastic interactions, corresponding to phonon creation and annihilation, respectively, are characterized by an energy transfer at a given momentum transfer Q , which corresponds to a particular location in the first Brillouin zone. The energy positions and the widths of the excitations are fitted by using a Lorentzian model function, convoluted with an experimentally determined energy resolution function, by standard χ^2 minimization (shown in Fig. 3).

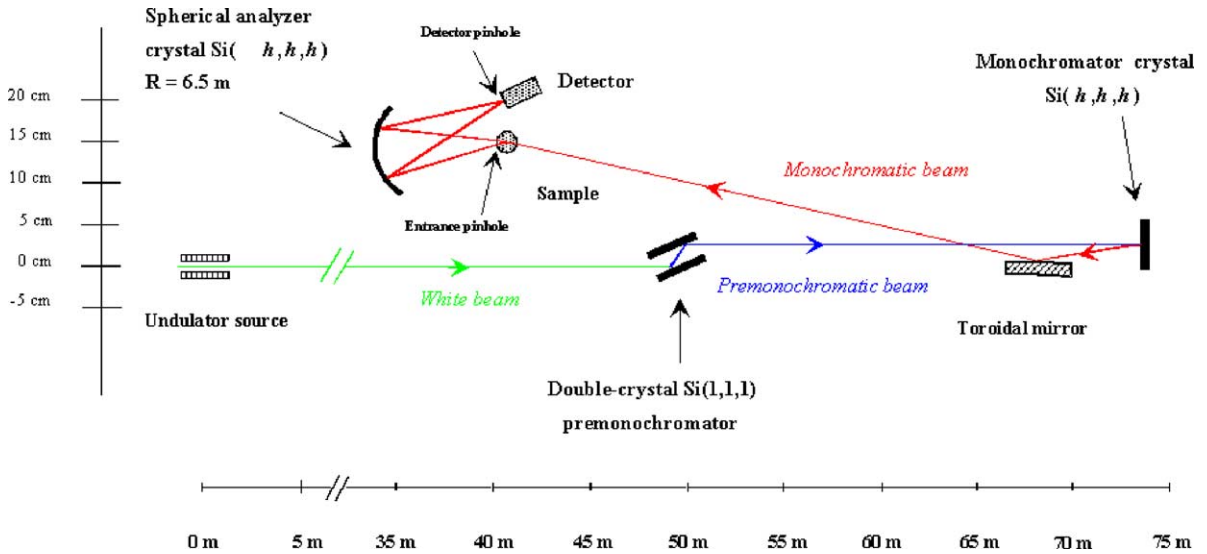


Fig. 2. Optical layout of ID28 beamline at ESRF (European Synchrotron Radiation Facility, Grenoble, France).

2.1. The example of iron and its implications for the Earth's inner core

The knowledge of the elastic constants of the phases of iron, which makes up 70–90 wt.% of planetary cores, is essential for comparison with global velocity models of Earth. The hcp (or ϵ) high-pressure phase is stable to at least 300 GPa at ambient temperature (Mao et al., 1990) and numerous experiments have

been carried out in order to characterize the elastic properties of iron phases, such as XRD (Mao et al., 1998; Matthies et al., 2001), NRIXS (Lubbers et al., 2000; Mao et al., 2001), or INS on the low pressure bcc phase (Klotz and Braden, 2000). As shown in Fiquet et al. (2001), IXS provides a way to derive the acoustic velocity from the dispersion of the longitudinal acoustic phonon energy in iron. The results of this study are used here for illustrating how acoustic velocities are obtained from IXS data collected under high pressure.

In this experiment, a polycrystalline sample of iron was loaded into the 120 μm hole of a rhenium gasket and compressed without any pressure transmitting medium between diamond anvils. In the following, only the Stokes part of the spectra has been collected to save time. The peak centered at zero-energy transfer corresponds to the elastic contribution to the signal, whereas two other peaks are visible at higher energy transfer. The knowledge of the phonon dispersion curves of iron (Minkiewicz et al., 1967) and diamond (Warren et al., 1967) allows an unambiguous assignment of these features, which correspond to a LA phonon of iron and a transverse acoustic TA phonon of diamond (see Fig. 4). With the five analyzers located in the horizontal plane at different scattering angles θ , it is possible to map the dispersion curves of acoustic phonons across the first Brillouin zone. Due

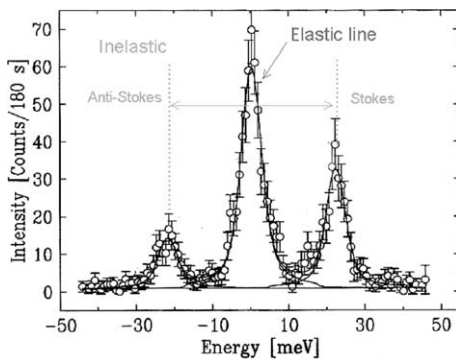


Fig. 3. Example of an inelastic X-ray scattering pattern obtained from a bcc iron foil at ambient conditions using the (888) monochromator reflection, providing an energy resolution of 5.5 meV. Scanning time is 5 h. $Q = 6.16 \text{ nm}^{-1}$. The experimental data (open circles) are plotted with their error bars along with the corresponding fits.

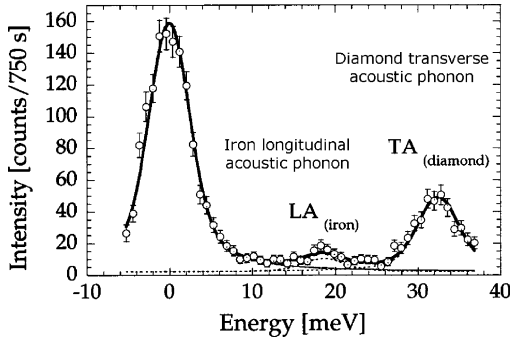


Fig. 4. IXS pattern recorded on a powdered iron sample in the hcp phase, at 28 GPa in a diamond–anvil cell. No pressure transmitting medium is used. The momentum transfer Q is 4 nm^{-1} . Dashed lines represent the inelastic contributions of the LA phonon branch for iron and from a TA branch from diamond, the thin solid line represents the elastic contribution and the thick continuous line shows the summation of individual contributions.

the polycrystalline nature of the sample, only modulus Q is defined, but not its direction. We consequently only record an orientationally averaged LA velocity. Furthermore, the inelastic scattering cross section is proportional to the dot product $(\vec{Q}\vec{e}_q)^2$ where \vec{Q} is the momentum transfer and \vec{e}_q is the phonon eigenvector of mode q (e.g. Ashcroft and Mermin, 1976). Consequently, only modes whose eigenvectors have a component parallel to \vec{Q} are visible in a coherent inelastic scattering experiment. For momentum transfers within the first Brillouin zone in polycrystalline systems, these modes are predominantly of longitudinal character (Burkel, 2000). However, transverse modes can be detected, though weaker in their intensity, due to the fact that along an arbitrary crystalline direction, there can be a non-zero contribution of the transverse phonon eigenvectors projected onto the momentum transfer direction. Indeed, weak detection of TA mode in iron is evidenced in Fig. 5 for some Q values. Furthermore, in some directions, some LA–TA mixing might occur, but as the intensity contribution of TA modes is weak, this effect is most likely negligible.

As shown in Fig. 5, different excitations corresponding to iron LA or TA phonons can be fitted at different Q values. The TA phonon of diamond visible at $Q = 4 \text{ nm}^{-1}$ disappears at higher Q values in the recorded energy transfer region because of its high sound velocity. The LA iron phonon branch is recorded over the entire momentum and pressure range explored, as

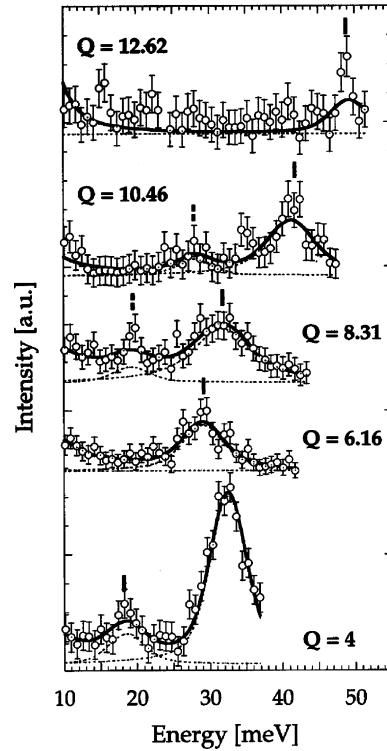


Fig. 5. IXS dispersion of the iron LA phonon recorded in the hcp phase of iron at 28 GPa. These patterns correspond to the signal recorded on the whole analyser set, i.e. at five different Q values. The LA phonons of iron are indicated by ticks. The excitation indicated by broken ticks for Q values at 8.31 and 10.46 nm^{-1} have been interpreted as a TA phonon in iron sample.

shown in Fig. 6 on the dispersion curves resulting from the fitted energy position of the phonon reported as a function of the momentum transfer Q . We notice that the high-pressure data are at energies well above those at ambient pressure, implying a significant increase of the sound velocity with increasing pressure, in the bcc phase as well as in the hcp phase of iron. The velocity of longitudinal acoustic velocity (V_P) as well as the position of the edge of the first Brillouin zone Q_{MAX} can be estimated by fitting the dispersion relation with a sine law, and by determining its slope in the $Q = 0$ limit with the following expression:

$$E[\text{meV}] = 4.192 \times 10^{-4} V_P[\text{ms}^{-1}] \times Q_{\text{MAX}}[\text{ns}^{-1}] \times \sin \left[\frac{\pi}{2} \frac{Q[\text{ns}^{-1}]}{Q_{\text{MAX}}[\text{ns}^{-1}]} \right] \quad (2)$$

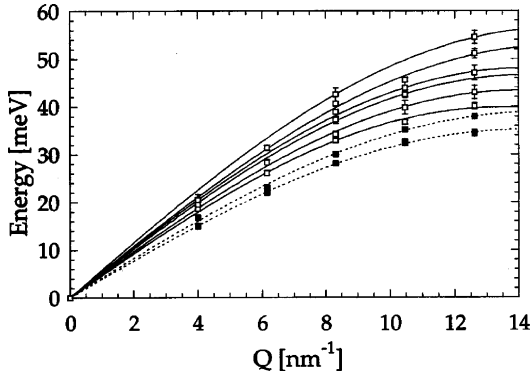


Fig. 6. Orientationally averaged dispersion curve of the longitudinal acoustic phonon branch of iron. The dashed line corresponds to data recorded in the bcc phase at 0.2 and 7 GPa, solid lines stand for fitted dispersion curves in the hcp phase of iron at pressures of 19, 28, 45, 55, 64 and 110 GPa from bottom to top.

The first Brillouin zone is approximated here by a sphere defined by radius Q_{MAX} , which has been considered as a free parameter in the fitting procedure. Within uncertainties, the observed values of Q_{MAX} calculated from XRD data by equating the volume of the reciprocal unit-cell to that of a sphere are in agreement with those obtained during the fit. Data recorded at four to five momentum transfers have been used in each dispersion curve to constrain V_P within an estimated error of 3%.

Our results for the low-pressure bcc structure agree within 1% with the ultrasonic data collected up to 1 GPa and extrapolated up to 10 GPa (Guinan and Beshers, 1968), thus confirming the reliability of these measurements (see Fig. 7). Results obtained in the hcp phase are given in Table 1 and reported as a function of pressure in Fig. 8, along with previous measurements obtained with other techniques. At low pressures (below 40 GPa), we find an excellent agreement between our longitudinal acoustic velocity V_P determination and orientationally averaged ultrasonic data (data point at 26.5 GPa in Mao et al., 1998). Up to 100 GPa, our measurements are within error bars in good agreement with radial X-ray diffraction (Mao et al., 1998) or NRIXS data (Mao et al., 2001), whereas theoretical calculations yield much higher velocities (Steinle-Neumann et al., 2001). In Fig. 9, we also show that hcp iron follows a Birch law (see Birch, 1963) for V_P , namely a linear dependence between com-

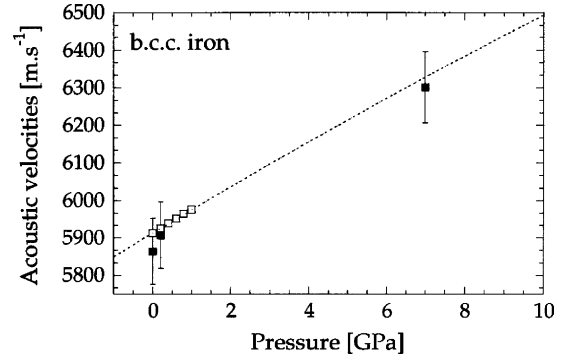


Fig. 7. Acoustic sound velocity as a function of pressure for bcc iron (solid squares) as compared to ultrasonics measurements and extrapolation by Guinan and Beshers (1968).

pressional sound velocity and density, which provides a convenient relationship for extrapolating our measurements to higher pressures. Furthermore, our measurements are in excellent agreement with the Hugoniot shock data of Brown and McQueen (1986) within the frame of the Birch's plot. These shock data have been collected at high temperature whereas our measurements have been carried out at ambient temperature. The important point is that both experiments yield the same observed acoustic velocity at a same given density, which is indeed the Birch assumption (Birch, 1963). It is striking to note that seismic data (Dziewonski and Anderson, 1981) does not fit the linear extrapolation made from the combination of the two sets of data. This could be interpreted as if Earth's

Table 1
Longitudinal acoustic sound velocities (m/s) as a function of specific mass (kg/m^3)

V_P	Specific mass	V_P	Specific mass
Iron		FeO	
7055	9084	6150	5770
7363	9382	6850	6000
7802	9861	7400	6360
8032	10107	7930	6600
8222	10315	8430	7147
8804	11229	8910	7270
		9160	7450
FeS ₂		FeSi	
8042	5010	7121	6239
8824	5277	8013	6630
9476	5492	9043	7293
10278	5757	9515	7507

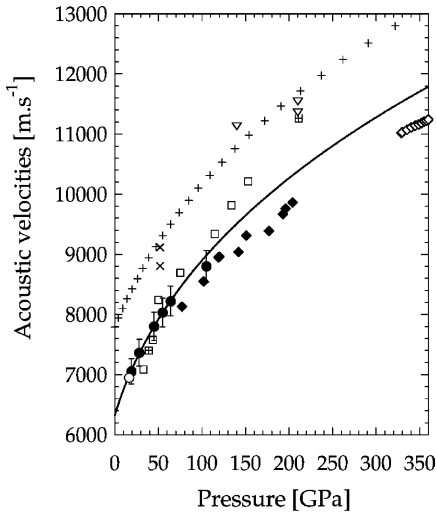


Fig. 8. Longitudinal acoustic sound velocity for the hcp phase of iron as a function of pressure (Fiquet et al., 2001: solid circles). Comparison is made with zero-frequency radial X-ray diffraction measurements (Singh et al., 1998: crosses; Mao et al., 1998: crossed squares), ultrasonics measurements (Mao et al., 1998: empty circle), nuclear resonance inelastic X-ray scattering (Mao et al., 2001: empty squares), Hugoniot sound velocity measurements (Brown and McQueen, 1986: solid diamonds), theoretical calculations (Stixrude and Cohen, 1995; Söderlind et al., 1996; Laio et al., 2000: empty triangles; Steinle-Neumann et al., 2001: small crosses) and PREM (Dziewonski and Anderson, 1981: empty diamonds).

inner core were 4–5% lighter than hcp iron, as previously suggested by Jephcoat and Olson (1987). Alternatively, this might indicate the presence of another phase of iron or alloy with different physical properties (e.g. Anderson, 1995). The comparison made with NRIXS data by Mao et al. (2001) shows that the extrapolations of the trends outside of the actual measurement ranges yield different values of V_P at inner core conditions, as well as different conclusions on the possible constitution of the inner core. In NRIXS experiments however, the determination of the average LA velocity is less direct than using IXS. The average Debye phonon velocity has to be extracted from a parabolic fit of the low-energy part of the density of states, and has to be converted into V_P and shear wave velocity V_S through an averaging scheme using independent determinations of bulk and shear moduli. Alternatively, such a difference between IXS and NRIXS results might originate in the way preferred orientations that develop at high pressure in diamond–anvil

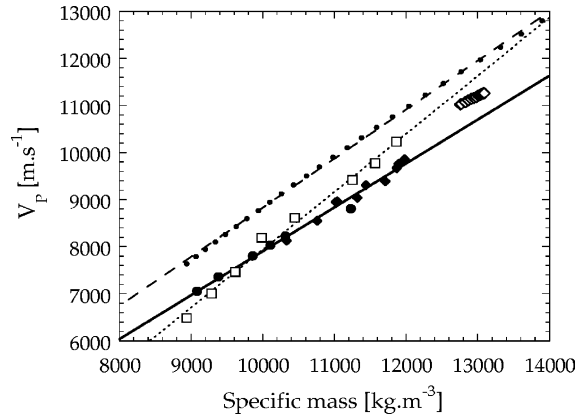


Fig. 9. Birch plot (i.e. the longitudinal acoustic velocity is represented as a function of specific mass) for hcp iron. Our inelastic X-ray scattering data (solid circles) and shock wave data (solid diamonds) closely follow a Birch law, a linear dependence of the longitudinal acoustic sound velocity with the specific mass, depicted by the solid line. Empty squares represent the results obtained by NRIXS (Mao et al., 2001) and the dashed line the associated Birch's fit made from these results only. Experimental observations are plotted along recent theoretical calculations (dots) by Steinle-Neumann et al. (2001).

cells in iron are taken into account. On a polycrystalline material, every single crystallite contributes to the total average LA dispersion curve. The average position and the width of LA excitation result from both the intrinsic resolution of the spectrometer and the sample texture. If orientation distribution is not random, the average might be biased toward velocities along that preferred orientation. XRD measurements carried out in parallel to our IXS study on the ID30 ESRF beamline indeed show that the c axis of iron is preferentially aligned with the compression axis of the diamond–anvil cell, in accordance with recently reported texture measurements (Wenk et al., 2000). Such measurements proposed in addition a large anisotropy for V_P , with P -waves travelling 8% faster at 45° from the c axis than either in the ab plane or along the c axis. According to these texture measurements, our IXS experiment probes mainly LA phonons propagating in the ab plane, since the momentum transfer lies approximately perpendicular to the incident X-ray beam and to the c axis. When anisotropy curves are considered however (see Wenk et al., 2000), the orientationally averaged V_P values we obtain from IXS are similar to the values corresponding to a predominant but not complete preferential orientation of the c axis.

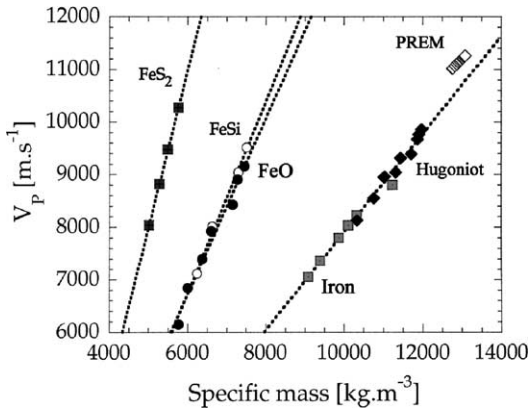


Fig. 10. Longitudinal acoustic sound velocity for iron-bearing compounds at high pressure, as compared to pure iron and the inner core sound velocity (open diamonds). Solid squares: pyrite; hollow circles: iron silicide; solid circles: iron oxide. Dashed lines are Birch's fits made to these observations.

In addition, we performed a series of measurements which show the influence of light elements such as sulfur, silicon or oxygen on acoustic sound velocities of iron alloys at high-pressure. The results are presented in Table 1 and reported as a function of specific mass in Fig. 10. One notices that iron silicide, iron oxide as well as pyrite closely follow a Birch's law, which provides an interesting way to extrapolate data at higher pressure and/or temperature and will therefore bring new constraints to the determination of the light elements content of the Earth's inner core (Badro et al., in preparation).

2.2. The investigation of the acoustic anisotropy of hcp metals at high-pressure: the example of cobalt

Beyond studies of the bulk properties of the Earth's core, seismological studies show that the inner core is elastically anisotropic (Woodhouse et al., 1986; Romanowicz et al., 1996; Song, 1997; Garcia and Souriau, 2000). The anisotropy has an axial symmetry and an amplitude of about 3%, with the fast direction oriented parallel to the Earth's rotation axis. Several hypotheses have been proposed to explain this feature: Jeanloz and Wenk (1988) proposed that the anisotropy might be caused by the lattice preferred orientation of the hcp structure of iron due to plastic deformation, whereas Karato (1993) invokes an in-

teraction of the Earth's magnetic field with growing magnetically anisotropic iron crystals. However, it is not clear whether hcp iron is highly anisotropic at very high pressure. Some theoretical results show a rather low intrinsic anisotropy, almost requiring a perfect alignment of iron hcp crystals in order to account for the observed seismic anisotropy (Stixrude and Cohen, 1995). More recent theoretical work shows that intrinsic anisotropy in hcp iron is of the order of 12% at inner core conditions and that perfect texturing is not required by the theoretical results (Steinle-Neumann et al., 2001). Texture X-ray diffraction measurements of iron at very high-pressure (Mao et al., 1998; Wenk et al., 2000) indicate a large compressional-wave anisotropy which relieves the "perfect alignment" textural constraint. This is illustrated in Fig. 11 where the longitudinal acoustic wave velocity is shown as a function of the direction of propagation for hcp iron. The anisotropy proposed by texture measurements (Mao et al., 1998), when compared to calculations (Stixrude and Cohen, 1995), is not only different in magnitude, but as well in direction. Conversely, the direction and magnitude of the anisotropy in another

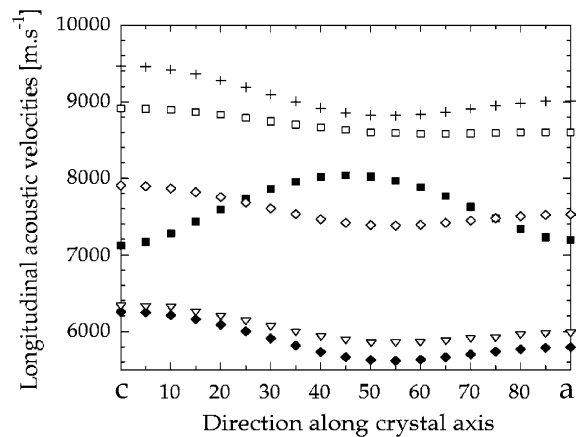


Fig. 11. Calculation of the anisotropy of propagation of longitudinal acoustic velocity for hcp iron and cobalt. Iron: zero-frequency radial X-ray diffraction measurements (solid squares) by Mao et al. (1998) compared at 39 GPa with first principles calculations (open squares) from Stixrude and Cohen (1995) and (crosses) from Steinle-Neumann et al. (2001). Cobalt: room pressure ultrasonics measurements (solid diamonds) by Guinan and Steinberg (1974) plotted along theoretical calculations (open triangles) from Steinle-Neumann et al. (1999). Calculations at 39 GPa are shown for hcp cobalt (open diamonds).

metal with hcp structure such as cobalt compare well (Guinan and Steinberg, 1974) with iron theoretical values.

In order to settle the above outlined discrepancies between the various indirect experimental techniques and theory, a direct experimental determination of the elastic constants of hcp iron and their evolution with pressure and temperature is needed. The key experiments would in fact be the direct comparison of single crystal and polycrystalline data in hcp-Fe. However, obtaining single crystals of hcp-Fe at high pressure is currently not possible. In the next paragraphs, we present preliminary results obtained on cobalt to address the issues of elastic anisotropy. Unlike iron, hcp cobalt is stable at room temperature and ambient pressure to 105 GPa (Yoo et al., 2000). Cobalt is a 3d transition metal located next to iron in the periodic table, and its bulk and thermal properties are close to those of iron. Thus, cobalt makes a good proxy for iron at high-pressure, and single crystals as well as powders can be obtained commercially. The example

we present here is focused on the determination of elastic moduli and their pressure derivatives. For the hcp structure there are five independent elastic moduli (C_{11} , C_{33} , C_{44} , C_{12} , C_{13}). These can be derived from the LA and TA phonon dispersion, fitted as shown previously with a sine function where the slope at $Q = 0$ yields acoustic velocities along main directions chosen by orientating the crystal kept at high-pressure in the diamond-anvil cell. With a single crystal with surface normal to $[1\ 1\ 0]$, it is possible to get C_{11} , C_{33} , C_{44} and C_{66} which are simply related to LA $[1\ 0\ 0]$, LA $[0\ 0\ 1]$, TA $[1\ 1\ 0]_{(001)}$ and TA $[1\ 1\ 0]_{(100)}$, respectively, whereas C_{12} can be easily obtained from $C_{66} = (1/2)(C_{11} - C_{12})$ and C_{13} is a linear combi-

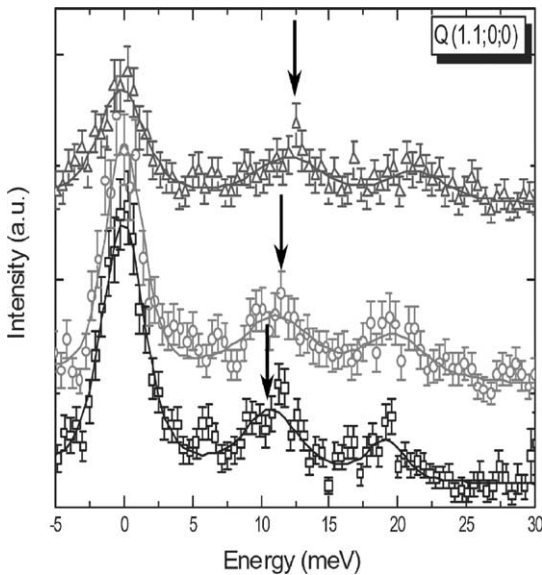


Fig. 12. IXS pattern collected on single crystal hcp cobalt at three different pressures in a diamond-anvil cell. Helium is used as pressure transmitting medium: Squares: 3.3 GPa, circles: 6.5 GPa, triangles: 9.5 GPa. The energy position of the LA phonon is indicated by the arrow. A higher energy phonon can be assigned to an optical mode. Reduced- Q setting is 1.1 along $[1\ 0\ 0]$ direction in hcp cobalt. The data were taken with an energy resolution of 3 meV.

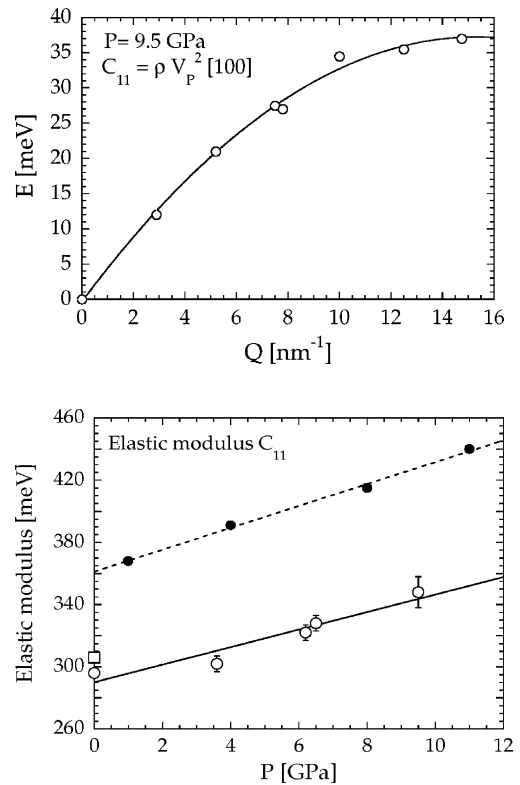


Fig. 13. Top: Dispersion curve of the longitudinal acoustic phonon branch along the $[1\ 0\ 0]$ direction in hcp cobalt at 9.5 GPa. Bottom: pressure dependence of C_{11} elastic modulus (open circles). Ultrasound measurements at room pressure (Landolt-Bornstein, 1966) appear as an open diamond whereas theoretical calculations by Steinle-Neumann et al. (1999) are represented by solid dots. Lines are linear fits to the data. The pressure derivative is 5.3 (4) and the extrapolation to room pressure is $C_{11} = 290 \pm 2$ GPa.

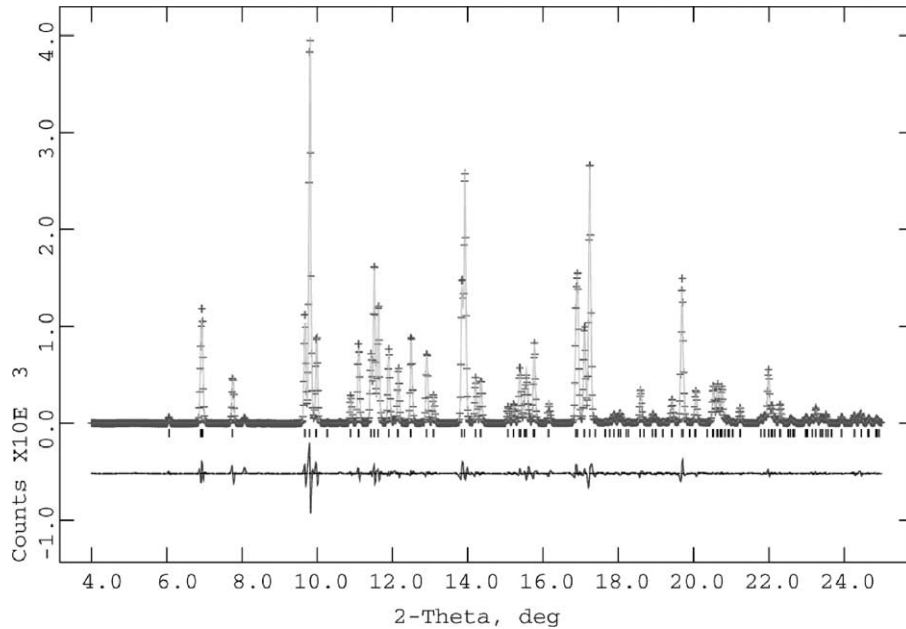


Fig. 14. X-ray diffraction pattern of synthetic MgSiO_3 with perovskite structure (space group $Pbnm$) with lattice parameters $a = 4.7765(1) \text{ \AA}$, $b = 4.9294(1) \text{ \AA}$, $c = 6.8977(1) \text{ \AA}$. The pattern has been obtained at a wavelength $\lambda = 0.41584 \text{ \AA}$ using an imaging plate located at 363.42 mm from the sample.

nation involving the other four elastic moduli. In order to reach the highest pressure we are aiming at (40–50 GPa), the crystal dimensions compatible with the constraints of the diamond anvil cell are 50 μm in diameter and 15 μm in thickness. These single crystals, which have to be of high quality, have been prepared at the Lawrence Livermore National Laboratory using state-of-the-art polishing and laser cutting techniques, and subsequently loaded in a diamond anvil cell using helium as a pressure transmitting medium. The first set of experiments presented here has been obtained on the ID28 beamline at ESRF using a single crystal with surface normal to [001]. Typical IXS pattern obtained at pressure up to 9.5 GPa are shown in Fig. 12. It allowed us to obtain the variation of the LA wave velocity along the [100] direction with increasing pressure. Combining these results with density measurements obtained by XRD, we obtain directly C_{11} and its variation with pressure as shown in Fig. 13, plotted along with recent theoretical determinations (Steinle-Neumann et al., 1999).

These investigations have recently been extended to determine the five elastic constants and their pressure

dependences to 42 GPa (Antonangeli et al., in preparation) and will be complemented by measurements on polycrystalline cobalt, in a manner similar to the experiments described above on iron. The sound ve-

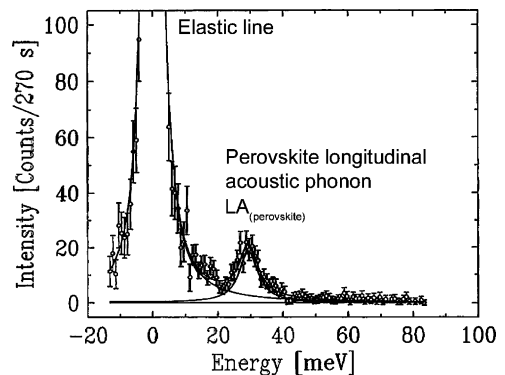


Fig. 15. IXS pattern collected at ambient conditions on a sintered polycrystalline sample of MgSiO_3 with perovskite structure with an energy resolution of 3 meV and at a momentum transfer of 4.5 nm^{-1} . The fits of the elastic line and the LA phonon (continuous lines) are plotted along with the experimental data.

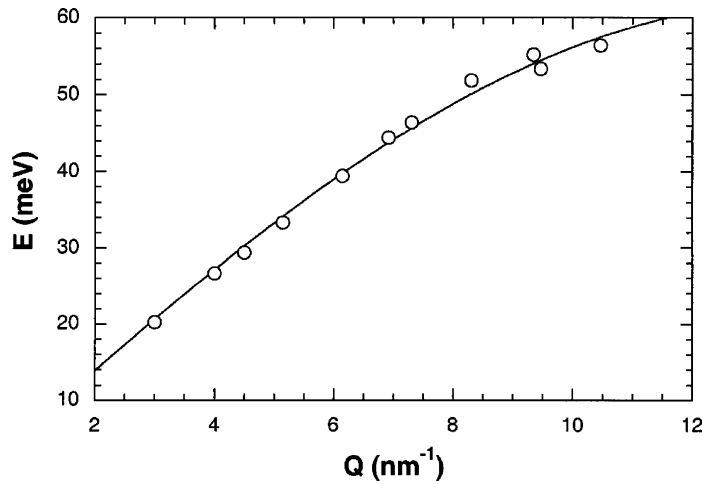


Fig. 16. Polycrystalline longitudinal acoustic phonon dispersion and corresponding sine function fit [Eq. (2)] for MgSiO_3 perovskite. The resulting mean longitudinal acoustic sound velocity is 10652 ± 173 m/s. The value of Q_{MAX} is a free parameter in this fit ($Q_{\text{MAX}} = 13.92 \pm 0.67 \text{ nm}^{-1}$).

locities obtained for the aggregate will be compared to the ones obtained by an orientational averaging of the single crystal data, in order to probe the accuracy of the averaging process. Moreover, we will obtain crucial data on the intrinsic anisotropy of sound velocity propagation in an hcp metal under pressure, and directly use it to estimate the anisotropy of iron at high-pressure.

2.3. Preliminary IXS data on magnesium silicate MgSiO_3 perovskite

Physical properties of MgSiO_3 with perovskite structure are of interest to better understand both the composition and current state of the Earth's lower mantle (670 to 2900 km in depth). The knowledge of the elastic constants of this compound, which makes

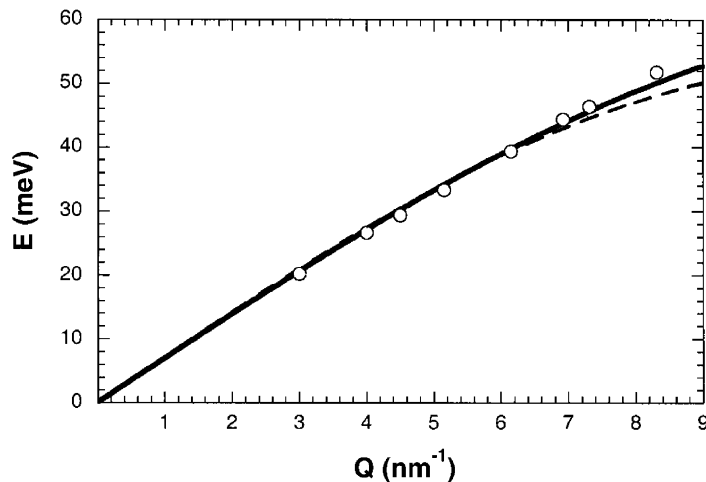


Fig. 17. Experimental measurements plotted along with different simulated dispersion curves calculated using Yeganeh-Haeri et al. (1989) elastic constants (with a Voigt-Reuss-Hill average of LA velocity of 10940 m/s) and different averaging processes. The solid line represents a fit with Q_{MAX} considered as a free parameter; the dashed line is calculated with a spherical first Brillouin zone.

up to 70–100 wt.% of the lower mantle, is essential for comparison with Earth's global seismic models, as well as to translate tomographic images into temperature and composition fields. It is also important to understand the lattice dynamics of this phase, which both determines its thermal properties at high pressure and temperature (e.g. Gillet et al., 2000) and which is related to possible phase transitions via soft-mode mechanisms (Hemley and Cohen, 1992; Wang et al., 1992).

In our preliminary experiment, a sintered sample of polycrystalline magnesium silicate perovskite was measured at ambient conditions. Further experiments will be carried out on MgSiO_3 single crystals, but there are some interesting points in proving that working on powders of silicate perovskite is possible. First, it is difficult to keep single crystals at very high pressures whereas powders can be compressed to pressures exceeding the 135 GPa of the core-mantle boundary. Second, IXS on a well sintered powder can still yield information about average acoustic velocities, which can be compared to geophysical models. Our experiments on MgSiO_3 perovskite were performed on a polycrystalline sample synthesized at the mineral physics institute of the State University of New York at Stony Brook. The sample was mounted on a glass fiber and checked by X-ray diffraction using a focused monochromatic radiation and imaging plate (MAR345) detector at the ID09 beamline of ESRF. We confirmed that the sample is a pure MgSiO_3 compound with perovskite structure, and no preferred orientations are detectable from the Rietveld refinement of the XRD pattern presented in Fig. 14. An example of an IXS spectrum is presented in Fig. 15, showing a well resolved LA mode of silicate perovskite. IXS data were collected at eleven different Q -settings, which allowed us to obtain the first experimental averaged dispersion curve in silicate perovskite with MgSiO_3 composition. Results are plotted in Fig. 16 along with the fit made using relation [2] in order to retrieve sound velocities. The results are $V_P = 10652 \pm 173$ m/s for the LA acoustic velocity and $Q_{\text{MAX}} = 13.92 \pm 0.67$ nm⁻¹. In Fig. 17, a simulated dispersion curve of orientationally averaged LA mode of silicate perovskite is also reported. The simulation has been made using elastic constants measured by Yeganeh-Haeri et al. (1989),

yielding a Voigt-Reuss-Hill average of (LA) velocity of 10940 m/s, and a spherical first Brillouin zone ($Q_{\text{MAX}} = 11.66$ nm⁻¹). As far as acoustic longitudinal velocity determination is concerned, the agreement between experimental and simulated curves is satisfactory. This is not the case for the parameter Q_{MAX} : above $Q = 6$ nm⁻¹, however, the IXS pattern is complicated by the dispersion curves of low frequency optical modes crossing the longitudinal acoustic dispersion curve near the zone edge (see theoretical calculations by Karki et al., 2000 or Parlinski and Kawazoe, 2000). The two curves in Fig. 17 show that the determination of sound velocity is not highly sensitive upon a detailed modeling of Q_{MAX} . In order to check for elastic anisotropy, simultaneous measurements of longitudinal phonons with 3D structure of the powder, as well as determination of ab initio calculated dispersion curves are needed for refining such determinations of average V_P in silicate perovskite.

3. Conclusions

Inelastic X-ray scattering is a well suited spectroscopic technique for the study of phonon dispersion of materials under high pressure. On both inelastic scattering beamlines of ESRF (ID16 and ID28), specific emphasis was given to high pressure. Moreover, the focusing optics scheme on ID28 is currently upgraded, and a focal spot size of 30 $\mu\text{m} \times 60 \mu\text{m}$ (horizontal \times vertical, FWHM) has been recently accomplished, thus enabling investigations on smaller samples, i.e. higher pressures. This work shows that a large variety of samples (metals or oxides) can be studied, either in a polycrystalline form (powders, sintered samples...) or as single crystals. Inelastic scattering experiments carried out on polycrystalline samples provide direct determination of orientationally averaged longitudinal acoustic sound velocities, whereas investigations on single crystals yield elastic moduli and a view on the dynamics of phase transitions. This technique is thus highly interesting for mineral physicists and offers a great potential in providing essential elastic data and their pressure and/or temperature dependence for most compounds of geophysical interest.

Acknowledgements

We thank Bernard Couzinet, Jean Claude Chervin, Bernard Canny for their assistance in diamond-anvil cell helium loading, and Matteo d'Astuto for their help on ID28 inelastic scattering beamline. Mohamed Mezouar and Michael Hanfland are acknowledged for their assistance with unscheduled X-ray diffraction sample characterization on high-pressure beamlines ID30 and ID09 of ESRF. Constructive reviews by L. Stixrude and an anonymous reviewer are appreciated.

References

- Abramson, E.H., Brown, J.M., Slutsky, L.J., 1999. Applications of impulsive stimulated scattering in the Earth and planetary sciences. *Annu. Rev. Phys. Chem.* 50, 279–313.
- Alfe, D., Price, G.D., Gillan, M.J., 2001. Thermodynamics of hexagonal-close-packed iron under Earth's core conditions. *Phys. Rev. B* 64 (45123), 1–16.
- Ashcroft, N.W., Mermin, N.D., 1976. *Solid State Physics*. Saunders College Publishing & Harcourt Brace College Publishers, Orlando, p. 826.
- Anderson, O.L., 1995. Mineral physics of iron and of the core. *Rev. Geophys. supplement*, 429–441.
- Birch F., 1963. In: Paul, W., Warschauer, D.M. (Eds.), *Solids Under Pressure*. McGraw-Hill, New York, pp. 137–162.
- Brown, J.M., McQueen, R.G., 1986. Phase transitions, Grüneisen parameter, and elasticity for shocked iron between 77 and 400 GPa. *J. Geophys. Res.* B 91 (7), 7485–7494.
- Brown, J.M., Slutsky, L.J., Nelson, K.A., Cheng, L.T., 1989. single-crystal elastic constants for San Carlos peridot: an application of impulsive stimulated Brillouin scattering. *J. Geophys. Res.* 95, 9485–9492.
- Burkel, E., Peisl, J., Dorner, B., 1987. Observation of inelastic X-ray scattering from phonons. *Europhys. Lett.* 3 (8), 957–961.
- Burkel, E., 2000. Phonon spectroscopy by inelastic X-ray scattering. *Rep. Prog. Phys.* 63 (2), 171–232.
- Chai, M., Brown, J.M., Slutsky, L.T., 1997a. The elastic constants of pyrope-grossular-almandine garnet to 20 GPa. *Geophys. Res. Lett.* 24, 523–526.
- Chai, M., Brown, J.M., Slutsky, L.T., 1997b. The elastic constants of an aluminous orthopyroxene to 12.5 GPa. *J. Geophys. Res.* 102, 14779–14785.
- Dorner, B., Burkel, E., Illini, T., Peisl, J., 1987. First measurement of a phonon dispersion curve by inelastic X-ray scattering. *Z. Phys. B Cond. Matter* 69 (2-3), 179–183.
- Duffy, T.S., Ahrens, T.J., 1992. Sound velocities at high pressure and temperature and their geophysical implications. *J. Geophys. Res.* B 97 (4), 4503–4520.
- Duffy, T.S., Ahrens, T.J., 1994. The temperature sensitivity of elastic wave velocity at high pressure; new results for molybdenum. *Geophys. Res. Lett.* 21 (6), 473–476.
- Duffy, T.S., Ahrens, T.J., 1995. Compressional sound velocity, equation of state, and constitutive response of shock-compressed magnesium oxide. *J. Geophys. Res.* 100 (B1), 529–542.
- Dziewonski, A.M., Anderson, D.L., 1981. Preliminary reference Earth model. *Phys. Earth Planet Int.* 25, 297–356.
- Fiquet, G., Badro, J., Guyot, F., Requardt, H., Krisch, M., 2001. Sound velocities in iron to 110 GPa. *Science* 291, 468–471.
- Garcia, R., Souriau, A., 2000. Inner core anisotropy and heterogeneity level. *Geophys. Res. Lett.* 27, 3121–3124.
- Gillet, P., Daniel, I., Guyot, F., Matas, J., Chervin, J.C., 2000. A thermodynamic model for MgSiO₃-perovskite derived from pressure, temperature and volume dependence of the Raman mode frequencies. *Phys. Earth Planet Int.* 117, 361–384.
- Guinan, M., Steinberg, D., 1974. *J. Phys. Chem. Solids* 35, 1501.
- Guinan, M.W., Beshers, D.N., 1968. Pressure derivatives of the elastic constants of iron to 10 kbs. *J. Phys. Chem. Solids* 29 (3), 541–549.
- Hemley, R.J., Cohen, R.E., 1992. *Ann. Rev. Earth Planet. Sci.* 20, 553–560.
- Isaak, D.G., Anderson, O.L., Goto, T., 1989a. Elasticity of single-crystal forsterite measured to 1700 K. *J. Geophys. Res.* 94, 5895–5906.
- Isaak, D.G., Anderson, O.L., Goto, T., 1989b. Measured elastic moduli of single-crystal MgO up to 1800 K. *Phys. Chem. Minerals* 16, 704–713.
- Jeanloz, R., Wenk, R., 1988. Convection and anisotropy of the inner core. *Geophys. Res. Lett.* 15, 72–75.
- Jephcoat, A., Olson, P., 1987. Is the inner core of the Earth pure iron? *Nature* 325, 332–335.
- Karato, S.-I., 1993. Inner core anisotropy due to the magnetic field-induced preferred orientation of iron. *Science* 262, 1708–1711.
- Karki, B.B., Wentzcovitch, R.M., de Gironcoli, S., Baroni, S., 2000. Ab initio lattice dynamics of MgSiO₃ perovskite at high pressure. *Phys. Rev. B* 62 (22), 14750–14756.
- Karki, B.B., Stixrude, L., Wentzcovitch, R.M., 2001. High-pressure elastic properties of major materials of Earth's mantle from first principles. *Rev. Geophys.* 39 (4), 507–534.
- Klotz, S., Braden, M., 2000. Phonon dispersion of bcc iron to 10 GPa. *Phys. Rev. Lett.* 85 (15), 3209–3212.
- Krisch, M., Mermet, A., San Miguel, A., Sette, F., Masciovecchio, C., Ruocco, G., Verbeni, R., 1997. Acoustic-phonon dispersion in CdTe at 7.5 GPa. *Phys. Rev. B* 56, 8691–8694.
- Laio, A., Bernard, S., Chiarotti, G.L., Scandolo, S., Tosatti, E., 2000. Physics of iron at Earth's conditions. *Science* 287, 1027–1030.
- Landolt-Bornstein, *Numerical Data and Functional Relationships in Science and Technology New Series. group III, vol. 1*, Springer, Berlin, 1966.
- Li, B., Chen, G., Gwanmesia, G.D., Liebermann, R.C., 1998. Sound velocity measurements at mantle transition zone conditions of pressure and temperature using ultrasonic interferometry in a multi-anvil apparatus, *Properties of Earth and Planetary Materials at High Pressure and Temperature. Geophysical Monograph* 101, AGU, Washington, DC, pp. 41–61.

- Li, B., Liebermann, R.C., Weidner, D.J., 2001. P - V - V_P - V_S - T measurements on wadsleyite to 7 GPa and 873 K: implications for the 410 km seismic discontinuity. *J. Geophys. Res.* 106 (B12), 30575–30591.
- Liebermann, R.C., Li, B., 1998. In: Hemley, R.J. (Ed.), *Elasticity at High Pressures and Temperatures. Reviews in Mineralogy*, pp. 459–492.
- Loa, I., Kunc, K., Syassen, K., Krisch, M., Mermet, A., Hanfland, M., 2003. Inelastic X-ray scattering in Cs under pressure. *High Pressure Res.* 23, 1–5.
- Lubbers, R., Grünsteudel, H.F., Chumakov, A.I., Wortmann, G., 2000. Density of phonon states in iron at high pressure. *Science* 287, 1250–1253.
- Mao, H.K., Wu, Y., Chen, L.C., Shu, J., Jephcoat, A.P., 1990. Static compression of iron to 300 GPa and $\text{Fe}_{0.8}\text{Ni}_{0.2}$ alloy to 260 GPa: implications for composition of the core. *J. Geophys. Res.* 95 (B13), 21737–21742.
- Mao, H.K., Shu, J., Shen, G., Hemley, R.J., Li, B., Singh, A.K., 1998. Elasticity and rheology of iron above 220 GPa and the nature of the Earth's inner core. *Nature* 396, 741–743; erratum: *Nature* 399, 280.
- Mao, H.K., Xu, J., Struzhkin, V.V., Shu, J., Hemley, R.J., Sturhahn, W., Hu, M.Y., Alp, E.E., Vočadlo, L., Alfe, D., Price, G.D., Gillan, M.J., Schwöerer-Böhning, M., Häusermann, D., Eng, P., Shen, G., Giefers, H., Lübbers, R., Wortmann, G., 2001. Phonon density of states of iron up to 153 GPa. *Science* 292, 914–916.
- Masciovecchio, C., et al., 1996. A perfect crystal X-ray analyzer with meV energy resolution. *Nucl. Instr. Methods. Phys. Res. B* 111, 181.
- Minkiewicz, V.J., Shirane, G., Nathans, R., 1967. Phonon dispersion relation for iron. *Phys. Rev.* 162 (3), 528–531.
- Occelli, F., Krisch, M., Loubeyre, P., Sette, F., LeToullec, R., Masciovecchio, C., Rueff, J.P., 2001. Phonon dispersion curves in an argon single crystal at high pressure by inelastic X-ray scattering. *Phys. Rev. B* 63, 224306, 1–8.
- Oganov, A.R., Brodholt, J.P., Price, G.D., 2001. The elastic constants of MgSiO_3 perovskite at pressures and temperatures of the Earth's mantle. *Nature* 411, 934–937.
- Parlinski, K., Kawazoe, Y., 2000. Ab initio study of phonons and structural stabilities of the perovskite-type MgSiO_3 . *Eur. Phys. J.* B16, 49–58.
- Romanowicz, B., Li X.D., Durek, J., 1996. Anisotropy in the inner core: could it be due to low order convection? *Science* 274, 963–966.
- Schülke, W., 1991. In: Brown, G., Moncton, D.E. (Eds.), *Handbook on Synchrotron Radiation*. North Holland Publishing Company.
- Sinelnikov, Y.D., Chen, G., Neuville, D.R., Vaughan, M.T., Liebermann, R.C., 1998. Ultrasonic shear wave velocities of MgSiO_3 perovskite at 8 GPa and 800 K and lower mantle composition. *Science* 281, 677–679.
- Singh, A.K., Mao, H.K., Shu, J., Hemley, R.J., 1998. Estimation of single-crystal elastic moduli from polycrystalline X-ray diffraction at high pressure: application to FeO and iron. *Phys. Rev. Lett.* 80 (10), 2157–2160.
- Sinogeikin, S.V., Bass, J.D., 2000. Single-crystal elasticity of pyrope and MgO to 20 GPa by Brillouin scattering in the diamond cell. *Phys. Earth Planet Int.* 120, 43–62.
- Sinogeikin, S.V., Bass, J.D., 2002. Elasticity of Majorite and a Majorite–Pyrope solid solution to high pressure: implications for the transition zone. *Geophys. Res. Lett.* 29 (2), 52–55.
- Söderlind, P., Moriarty, J.A., Wills, J.M., 1996. First-principles theory of iron up to earth-core pressures: structural, vibrational and elastic properties. *Phys. Rev. B* 53 (21), 14063–14072.
- Song, X., 1997. Anisotropy of the Earth's inner core. *Rev. Geophys.* 35 (3), 297–313.
- Steinle-Neumann, G., Stixrude, L., Cohen, R.E., Gülseren, O., 2001. Elasticity of iron at the temperature of the Earth's inner core. *Nature* 413, 57–60.
- Steinle-Neumann, G., Stixrude, L., Cohen, R.E., 1999. First-principles elastic constants for the hcp transition metals Fe, Co, and Re at high pressure. *Phys. Rev. B* 60 (2), 791–799.
- Stixrude, L., Cohen, R.E., 1995. High-pressure elasticity of iron and anisotropy of Earth's inner core. *Science* 267, 1972–1975.
- Stixrude, L., Cohen, R.E., Hemley, R.J., 1998. Theory of minerals at high pressure. In: Hemley, R.J. (Ed.), *Reviews in Mineralogy*. vol. 37, pp. 639–671.
- Verbeni, R., Sette, F., Krisch, M.H., Bergmann, U., Gorges, B., Halcoussis, C., Martel, K., Masciovecchio, C., Ribois, J.F., Ruocco, G., Sinn, H., 1996. X-ray monochromator with 2×10^{-8} energy resolution. *J. Synchrotron Radiat.* 3, 62.
- Wang, Y., Guyot, F., Liebermann, R.C., 1992. Electron microscopy of $(\text{Mg,Fe})\text{SiO}_3$ perovskite: evidence for structural phase transitions and implications for the lower mantle. *J. Geophys. Res.* 97 (B9), 12327–12347.
- Warren, J.L., Yarnell, J.K., Dolling, G., Cowley, R.A., 1967. *Phys. Rev.* 158, 805.
- Wenk, H.R., Matthes, S., Hemley, R.J., Mao, H.K., Shu, J., 2000. The plastic deformation of iron at pressures of the Earth's inner core. *Nature* 405, 1044–1047.
- Woodhouse, J.H., Giardini, D., Li, X.D., 1986. Evidence for inner core anisotropy from free oscillations. *Geophys. Res. Lett.* 13, 1549–1552.
- Yeganeh-Haeri, A., Weidner, D.J., Ito, E., 1989. Elasticity of MgSiO_3 in the perovskite structure. *Science* 243, 787–789.
- Yoo, C.S., Cynn, H., Soderlind, P., Iota, V., 2000. New beta(fcc)-cobalt to 210 GPa. *Phys. Rev. Lett.* 84 (18), 4132–4135.
- Zaug, J., Abramson, E.H., Brown, J.M., Slutsky, L.J., 1993. Sound velocities in olivine at Earth mantle pressure. *Science* 260, 1487–1489.
- Zha, C.-S., Mao, H.K., Hemley, R.J., Duffy, T.S., Meade, C., 1994. Acoustic velocities and refractive index of SiO_2 glass to 57.5 GPa by Brillouin scattering. *Phys. Rev. B* 50, 13105–13112.
- Zha, C.-S., Mao, H.K., Hemley, R.J., 2000. Elasticity of MgO and a primary pressure scale to 55 GPa. *Proc. Natl. Acad. Sci. U.S.A.* 97 (25), 13494–13499.